COUPLED ANALYSIS USING 3D-CFD AND CHEMICAL MODEL FOR CORROSION AND SCALING OF TWO PHASE FLOW WELLBORE/PIPELINE

Kazumi Osato[1], Masatake Sato[1], and Kaichiro Kasai[1]

[1]Geothermal Energy Research and Development Co., Ltd.

osato@gerd.co.jp , msato@gerd.co.jp , kasai@gerd.co.jp

Keywords: CFD, *Software, Corrosion, Scaling, Chemistry, Risk Based Assessment, Geothermal*

ABSTRACT

Coupled analysis using three dimensional CFD (computed Fluid Dynamics) simulation model by the open source CFD code "OpenFOAM" with parallel computing and a wellbore chemical simulator "WellCHEM" (White et al, 2000) demonstrated the fact that could calculate two phase flow and chemical phenomena including corrosion and scaling of geothermal production wells and surface pipelines. This paper aims to discuss recent attempts of comparison between computed models and field data to predict the corrosion and scaling problems of geothermal production wells and pipelines. An acidic production well or a corroded horizontal pipeline with rising gradient was modeled by coupled analysis using 3D-CFD and "WellCHEM" in this paper. It was confirmed that domain of the steam with the moisture with the concentration of the chemical ingredient in wellbore casing/pipeline was changed by various flow conditions of geothermal fluid. This research was conducted under NEDO's contract research - "Research and Development of Geothermal Power Generation Technology".

1. INTRODUCTION

Recent attempts to combine software programs for corrosion and scaling tasks related to geothermal energy application has been discuss to provide interpreted advice (Lichti K. et al, 2005). This paper shows the combination of software for coupled analysis based three packages (Figure 1): GFLOW a wellbore simulator (Kato et al, 2001, Sato et al, 2003).WellCHEM for chemistry simulation (White et al, 2000). GeoPOUR for equilibrium Pourbaix corrosion product stability diagram (Lichti et al, 2005).

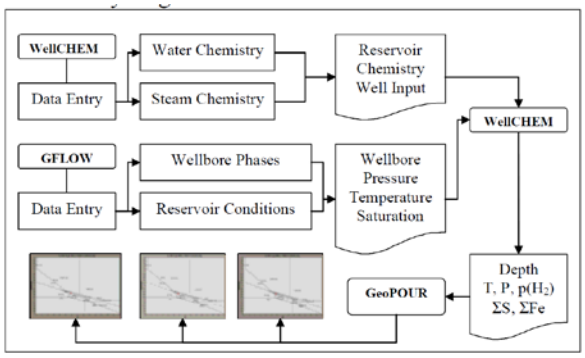

Figure 1: Process Flow Diagram for WellCHEM, GFLOW Plus GeoPOUR software (Lichti et al, 2005)

GFLOW is the wellbore simulator based on based on GWELL (Aunzo et al., 1991), whose source codes are available tothe public (Kato et al., 2001). In GFLOW, the following equations, functions, etc. are added to the existing correlations of Orkiszewski: Miller's correlation (Miller, 1979), CO_2 and NaCl simultaneous processing function, super-critical area calculation function, and a user interface (Kato et al., 2001). For high-inclined directional well, the applicable correlation equation is not included in GFLOW, and this may create an error in the pressure loss calculation. Thus, in order to develop a wellbore simulator applicable to highly-inclined directional well, the introduction of a Drift flux model has been studied (Kato et al., 2015). However, this simulator is based on one-dimension model along wellbore and homogenous in casing cross section. Since the phenomenon of corrosion and scaling occur concentration irregularity on inner surface of the pipe depended on various flow conditions, we need to calculate more detail by three-dimensional model.

OpenFOAM is a free, open source CFD software developed primarily by OpenCFD Ltd since 2004, distributed by OpenCFD Ltd and the OpenFOAM Foundation. It has a large user base across most areas of engineering and science, from both commercial and academic organizations. OpenFOAM has an extensive range of features to solve anything from complex fluid flows involving chemical reactions, turbulence and heat transfer. OpenFOAM is based on a free and open source C++ toolbox for the development of numerical solvers in continuum mechanics. We replaced GFLOW process of Figure 1 to OpenFOAM three dimensional CFD (3D-CFD) model (Figure 2).

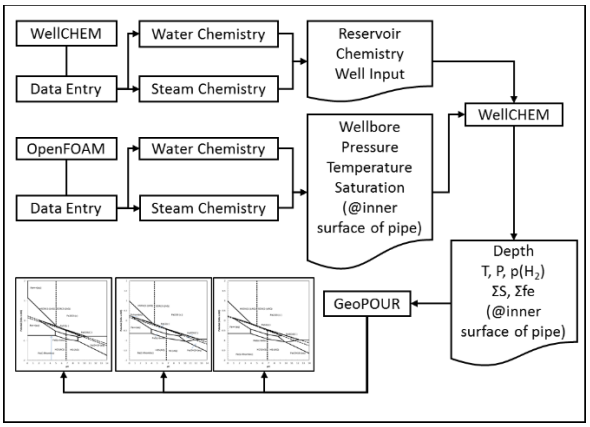

Figure 2: Process Flow Diagram for WellCHEM, OpenFOAM 3D-CFD Plus GeoPOUR software

2. OPENFOAM THREE DIMENSIOAL CFD

Eulerian multiphase model of OpenFAOM 2.3.0 was used for this study.

2.1 Basic equation (Jasak et al, 2007)

Law of conservation of mass;

$$\frac{\partial \alpha_i \rho_i}{\partial t} + \nabla \cdot (\rho_i \alpha_i \vec{U}_i) = 0 \quad (1)$$

Law of conservation of momentum;

$$\frac{\partial \alpha_i \vec{U}_i}{\partial t} + \nabla \cdot (\alpha_i \vec{U}_i \vec{U}_i) - \vec{U}_i \left(\frac{\partial \alpha_i}{\partial t} + \nabla \cdot (\alpha_i \vec{U}_i) \right) = -\frac{\nabla p}{\rho_i} + \nabla \cdot \tau_i + \vec{g} + \frac{\vec{F}_{Dji}}{\rho_i} + \frac{\vec{F}_{VMji}}{\rho_i} \quad (2)$$

p : Pressure of mixed phase

: Stress, $\tau_i = \left((\nu_i + \nu_t) \nabla \vec{U}_i \right) + \left((\nu_i + \nu_t) \nabla \vec{U}_i^{\,T} - 1/3 I \nabla \cdot \vec{U}_i \right)$ (3)

$\vec{F}_{Dji}$: Resistance of phase(i) influenced by phase(j)

$\vec{F}_{VMji}$: Virtual mass force (Inertial force) of phase(i) influenced by phase(j)

Turbulence model is mixing k-ε model;

$$\frac{\partial \rho_m k}{\partial t} + \nabla \cdot (\rho_m \vec{U}_m k) = \nabla \cdot \left(\left(\mu + \frac{\mu_t}{\sigma_k} \right) \nabla k \right) + P_{km} - \rho_m \varepsilon$$

$$\frac{\partial \rho_m \varepsilon}{\partial t} + \nabla \cdot (\rho_m \vec{U}_m \varepsilon) = \nabla \cdot \left(\left(\mu + \frac{\mu_t}{\sigma_\varepsilon} \right) \nabla \varepsilon \right) + \frac{k}{\varepsilon} (C_{1\varepsilon} P_{\varepsilon m} - C_{2\varepsilon} \rho_m \varepsilon) \quad (4)$$

$$\mu_t = C_\mu \rho_m \frac{k^2}{\varepsilon}$$

k : turbulent kinetic energy of mixing phase

ε : dissipation rate of mixing phase

$\rho_m = \Sigma \rho_i \alpha_i$: density of mixing phase

$U_m = \Sigma \rho_i \alpha_i U_i / \Sigma \rho_i \alpha_i$: mixing phase velocity (Mass-weighted average)

2.1 Equation of State

Law of conservation of mass;

Vaper phase is calorically perfect gas;

$$\rho_V = \frac{p}{R_V T_V} \quad (5)$$

T_V : Temperature [K]

R_V : Gas constant, R_V = 405.83 [J/kg/K]

Water is Non-compressible fluid;

$\rho_W = 841.7751$ [kg/m^3]

Volume fraction;

$$\delta = \frac{\alpha_V \rho_V}{\alpha_V \rho_V + (1-\alpha_V)\rho_W} \Rightarrow \quad \alpha_V = \frac{\delta \rho_W}{(1-\delta)\rho_V + \delta \rho_W} \quad (6)$$

δ : Dryness

Eulerian multiphase model defines continuous phase and dispersed phase. In this condition, water particles (droplet) disperse in continuous vaper phase.

Particle diameter of liquid;

$$\alpha_W = \frac{n\pi/6d^3}{V_C} \quad (7)$$

Here,

n : particle numbers of a cell, d : particle diameter, V_C : volume of a cell

$n = 1$, $V_c = 1\times10^{-8}$ [m^3] $\Rightarrow$ $d = 4\times10^{-4}$ [m],

However, we decided to use $d = 1\times10^{-4}$ [m] by reason of stability of the solution at start point.

Regarding momentum exchange between vaper phase and water phase, the resistance based on Schiller-Neumann's low and virtual mass based on constant model.

Regarding heat transfer, the convection heat transfer based on Ranz-Marshal's low.

2. NUMERICAL MODEL FOR OPENFOAM 3D-CFD

2.1 Test model and grid

We attempted to model the section of deviated wellbore (inclination = 45.2 [degrees]) based on a real production well. The model is liner-hunger section (6 meters) between 7" OD (ID =0.16[m]) slot-liner casing (L=2 [s]) and 9-5/8" OD (ID=0.22[m]) cemented casing (L=4[m]). Figure 3 shows the wellbore model.

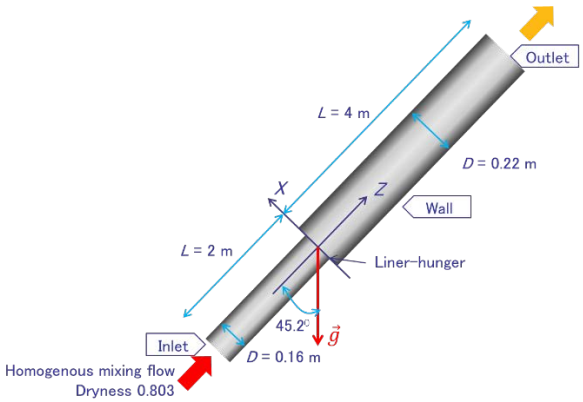

Figure 3: Wellbore Model for test

The modelling grid composed a half cylinder from 604,000 cells based hexahedral. The wall (inner surface of casing) section and liner-hunger section was modelled by more detailed cell (Figure 4).

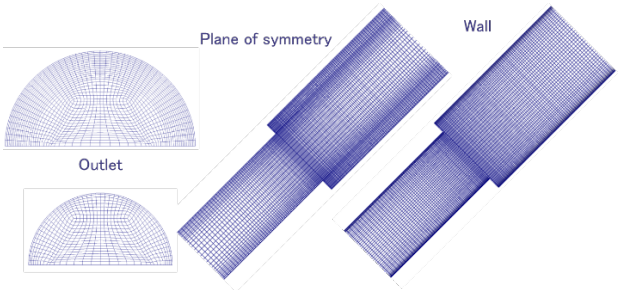

Figure 4: Modelling grid

2.2 Calculation

The solver is twoPhaseEulerFoam solver of OpenFOAM 2.3.0. Unsteady states, tree dimension, water-vaper two

phase flow, compressible vaper fluid and non-compressible water fluid, Eulerian multiphase model and mixing k-ε turbulence model were adopted in this study.

Property values and boundary conditions are shown in Table 1.

Table 1: Property values and boundary conditions

Property values	(Value)	(unit)
Vaper specific heat at constant pressure Cp_v	Steam table (Interpolation formula)	[J/kg/K]
Vaper viscosity μ_v		[Pa·s]
Vaper density ρ_v		[kg/m^3]
Water specific heat at constant pressure Cp_w		[J/kg/K]
Water viscosity μ_w		[Pa·s]
Water density ρ_w		[kg/m^3]
Boundary condition (Inlet)	(Value)	(unit)
Vaper volume fraction α_v	0.9967	-
Vaper temperature T_v	491.93	[K]
Vaper Pressure P_v	Zero gradient	[Pa]
Vaper mass flow $\dot{m}_v$*	2.925	[kg/s]
Water volume fraction α_v	0.0033	-
Water temperature T_w	491.93	[K]
Water Pressure P_w	Zero gradient	[Pa]
Water mass flow $\dot{m}_w$*	0.715	[kg/s]
Boundary condition (wall)	(Value)	(unit)
Volume fraction	Zero gradient	-
Temperature	Thermal insulation	[K]
Pressure	Zero gradient	[Pa]
Mass flow	Non-slip, Zero	[kg/s]

*Since the grid model is a half cylinder, mass flow is 1/2.

Figure 5 shows disturbance error between inlet mass flow rate and outlet mass flow rate (the horizontal axis is elapsed time [s]). Since average velocity was 12.75 [m/s] and length is 6 [m], one flow turnover by 0.5 [s]. 12 turnovers of the unsteady analysis were attempted in this calculation (total time = 6[s]). Since vaper phase was compressible flow and water is non-continuum model, inlet mass flow was not equal to outlet mass flow. However, if unsteady state moves to quasi-steady state, two mass flow values will move to close same values. The vertical axis of Figure 4 was no dimensionless value standardized by inlet flow value. When elapsed time will turn over 2 [s], the simulation changed to quasi-steady state condition.

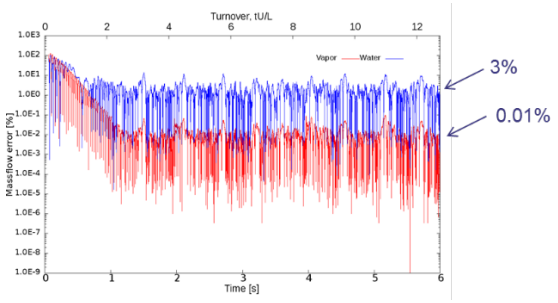

Figure 5: Disturbance error transition of calculated outlet water and vaper mass flow rate standardized by inlet mass flow rate

Figure 6 shows average (t=2[s] to 6[s]) velocity (z-direction) of vaper (upper coloured distribution) and water (lower coloured distribution). At section A (D=0.16[m]), vaper density was almost constant and average vaper velocity <<Uz_{vapor}>> was almost constant too. Average water velocity <<Uz_{water}>> was follow to vaper velocity because of resistance of small water particles. At section B (liner-hunger section), total average velocities <<Uz>> reduced due to expansion of wellbore diameter from 0.16[m] to 0.22[m]. <<Uz_{vapor}>> was almost constant. By the effect of peeling circulating flow, high velocity area of B section moves to contraction flow jet and accelerated. Since water particles are existing in this contraction flow jet, <<Uz_{water}>> was larger than <<Uz_{vapor}>>. This contraction flow jet was shifted to lower part by the effect of gravity. By this phenomenon, high velocity flow collides at an angle.

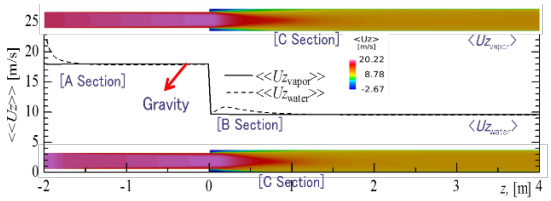

Figure 6: Average velocity (z direction) [m/s]

Figure 7 shows average pressure <<p>>. Average pressure change between inlet and outlet was only 0.1%. At the same diameter section, <<p>> was reduced by pressure loss. At the expansion section, static pressure transfer to dynamic pressure and <<p>> was increased. Since high velocity flow due to shifted contraction flow jet collides at an angle, pressure increased lower part of C section.

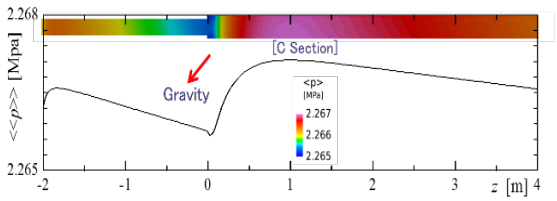

Figure 7: Average pressure [MPa]

Figure 8 shows average temperature <<T>>. Average pressure change between inlet and outlet was only 0.1%. <<T>> change was trend of reverse of <<Uz>> (Figure 6). Reduction of kinetic energy due to reduction of velocity at the expansion section increased vaper temperature due to

transfer to thermal energy by vaper compressibility. Water particle temperature followed to vaper temperature. Since diameter of water particles was small and specific surface area was larger, convection heat transfer between vaper and water was larger.

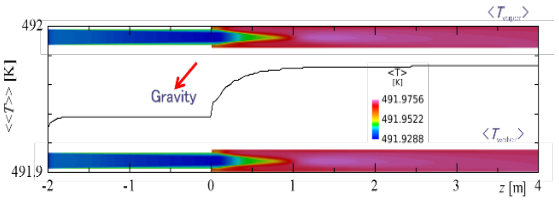

Figure 8: Average temperature [K]

Figure 9 shows average dryness <<dryness>>and volume fraction of vaper<< α_{vaper}>>. <<dryness>> was 0.8 – 0.9 but minimum <dryness> was only 0.2. In peeling circulation area at B section, since vaper phase was existing but water phase was almost not existing, both <dryness> and < α_{vaper}> increased. The contraction flow jet was shifted to lower part by the effect of gravity. By this phenomenon, high velocity flow collided at an angle and water particles were collected to lower wall of the pipe (z=2m, 3m, Outlet) (Figure 10). If water phase traps the majority of dissolved chemicals, corrosion and scaling will be accelerated in this section.

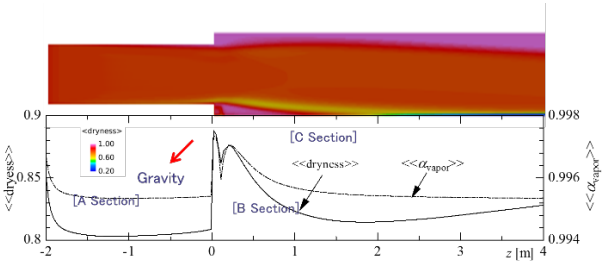

Figure 9: Dryness and volume fraction of vaper

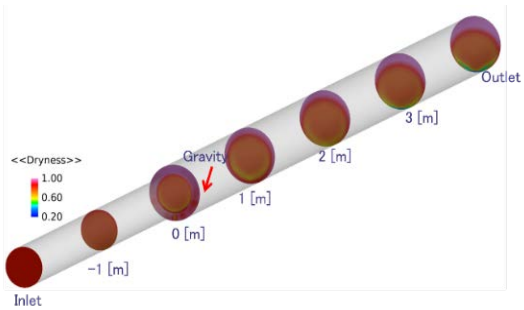

Figure 10: Dryness distribution of the pipe sections

Figure 11 shows vaper velocity of circumference direction at Inlet, -1[m], Expansion (Liner-hunger) 0 [m], 2[m], 3[m], and Outlet. At upstream section (D=0.16m), the circumference direction (X, Y) vectors were very small and the Axial (Z) vectors were main. However, at downstream section (D=0.22m), the cylindrical vectors were larger and vaper velocity has downward vector due to the effect of gravity to water particles.

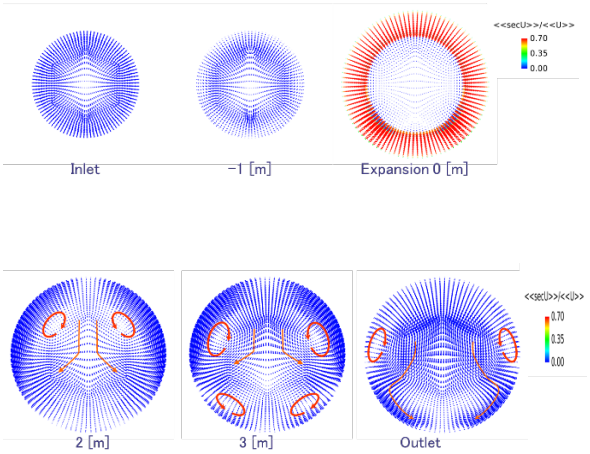

Figure 11: Vaper velocity (circumference direction) of each pipe sections [m/s]

Figure 12 shows instantaneous water velocity (z direction = wellbore direction) at 6 seconds (Uz_{water}(6[s])), average (<Uz_{water}>), residual error (Uz_{water}(6[s])- <Uz_{water}>). The disturbance occured at peeling shear layer of the casing show's downstream and the disturbance velocity from maximum velocity (|Uz_{water}|) was 18.8%. Since the velocity gradient and turbulent intensity were larger, water (particle dispersed phase) was a large freedom degree in movement and its turbulent speed increased. The peeling shear layer at lower part was more disturbed than upper part because water particles moved to lower part and increased disturbance.

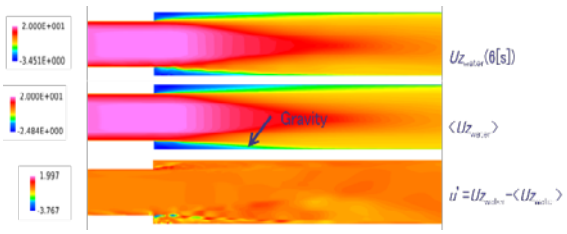

Figure 12: Instantaneous water velocity (z direction) [m/s]

Figure 13 shows instantaneous vaper velocity (z direction = wellbore direction) at 6 seconds, average, Residual error (6 [s] – average). The disturbance occurred at peeling shear layer of the casing show's downstream and the disturbance velocity from maximum velocity (|Uz_{vaper}|) was 6.5% and smaller than 18.8% at water phase because vaper phase was continuum phase and its turbulent speed was not easier to increase than water phase. This disturbance of vaper phase was due to the disturbance of water phase.

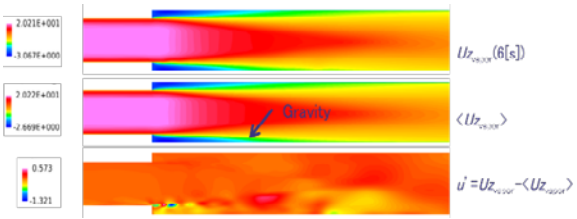

Figure 13: Instantaneous vaper velocity (z direction) [m/s]

Figure 14 shows instance pressure at 6 second and average and residual error (6 [s] – average). The disturbance of the peeling shear layer was 0.01% and only at the lower section.

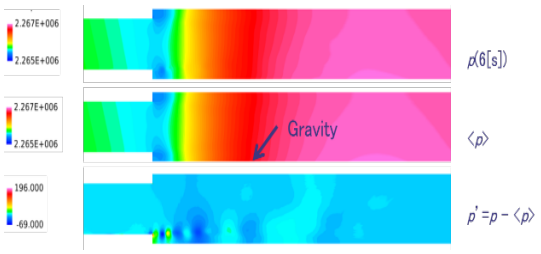

Figure 14: Instantaneous pressure [Pa]

Figure 15 shows instantaneous vaper temperature at 6 second and average and residual error (6[s] – average). The disturbance of the peeling shear layer was only 0.003%.

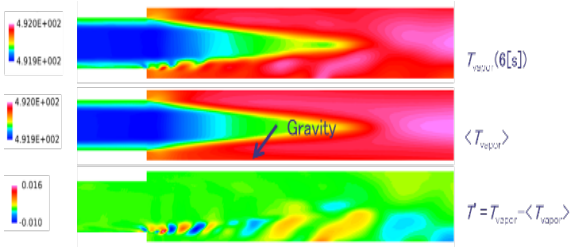

Figure 15: Instantaneous vaper temperature [K]

Figure 16 shows instantaneous water temperature at 6 second and average and residual error (6[s] – average). The disturbance of the peeling shear layer was only 0.003%.

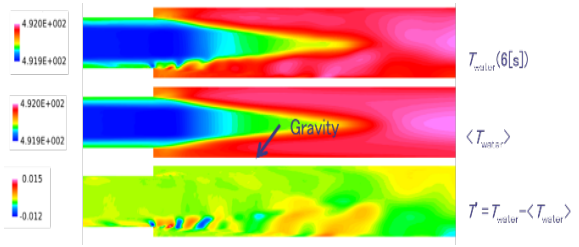

Figure 16: Instantaneous water temperature[K]

Figure 17 shows instantaneous vaper volume fraction at 6 second and average and residual error (6[s] – average). The disturbance of the peeling shear layer was 2.4%.

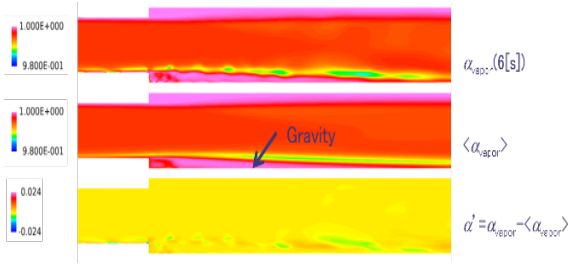

Figure 17: Instantaneous vaper volume fraction

Figure 18 shows instantaneous water volume fraction at 6 second and average and residual error (6[s] – average). The disturbance of the peeling shear layer was 32%. Since absolute value of water volume fraction was smaller, the disturbance was larger relatively.

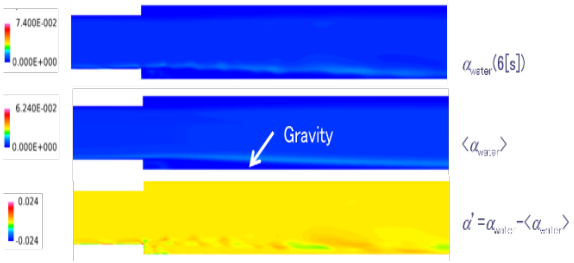

Figure 18: Instantaneous water volume fraction

3. CASE STUDY (PRODUCTION WELL)

We compared GFLOW calculation to OpenFOAM calculation in case of a deviated production well (inclination =34 [deg.]) in Japan. The bottom well condition is P=9.554[MPa], T=233.29[deg.C], and liquid phase condition. Figure 19 shows pressure, temperature, dryness, inclination and wellbore diameter profiles along the wellbore. In case of OpenFOAM, pressure <<P>> and temperature <<T>> is average value of each depth section, and dryness is upper side of the casing <Dryness (upper)> and lower side of the casing <Dryness (lower)>. The profiles were matched schematically but pressure and temperature were out of alignment in preparation for wellhead by degrees. We think that water particle diameter and heat transfer condition of wall have not optimized yet. We confirmed <Dryness (upper)> was larger than <Dryness (lower)> in the section of two phase flow and highly inclination. This phenomena is explained by the phenomena of Figure 9.

4. CASE STUDY (TWO-PHASE FLOW PIPELINE)

We tried to use OpenFOAM simulator in case of a surface two-phase flow pipeline with some bending parts and slope (5-10 degrees) in Japan. Figure 20 shows the birds-eye view of inner face dryness distribution of the pipeline. Using OpenFOAM result (pressure, temperature, dryness, and e nthalpy (water/steam)) and chemical analysis of brine and steam, we tried to use WellCHEM along the bottom line of the pipeline. Figure 21 shows Dryness calculated OpenFOAM and pH calculated by WellCHEM. At x=43m, we found the sections that were lower than pH4.5. Since the steam field operator found out the corrosion along the bottom of inner face pipe in the section (x=34m~43m) our simulation was harmonic to the field observation.

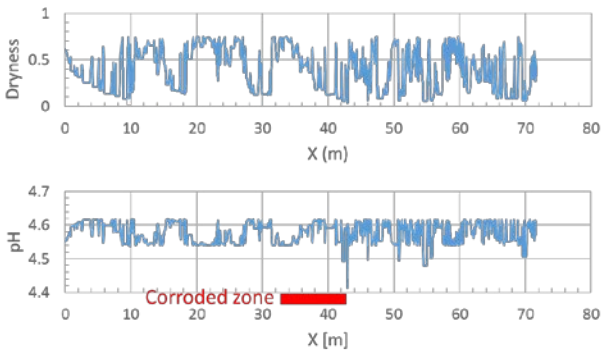

Figure 21: Dryness (every 0.01m) simulated by OpenFOAM 3D-CFD and pH (every 1 m) simulated by WellCHEM with OpenFOAM result on bottom line of the pipeline

Observed corroded section was positioned upstream of the lowest pH point (at x=43m) simulated by coupled analysis using OpenFOAM 3D-CFD and WellCHEM. Since this section had 5 degrees upward slope, we surmised that the water droplet in the bottom of the pipeline flowed back to upstream section for a long stretch of plant operation time and the simulator has not duplicated this phenomena yet.

Figure 22 shows Pourbaix diagrams of H_2S-H_20-Fe system in the bottom of pipe at x=42.95m. The condition at x=42.95m is still under passive film zone but near to corrosive zone. Since WellCHEM is a steady state simulation and cannot treat the condition of unsteady state, it might not been able to successfully pin-point calculation.

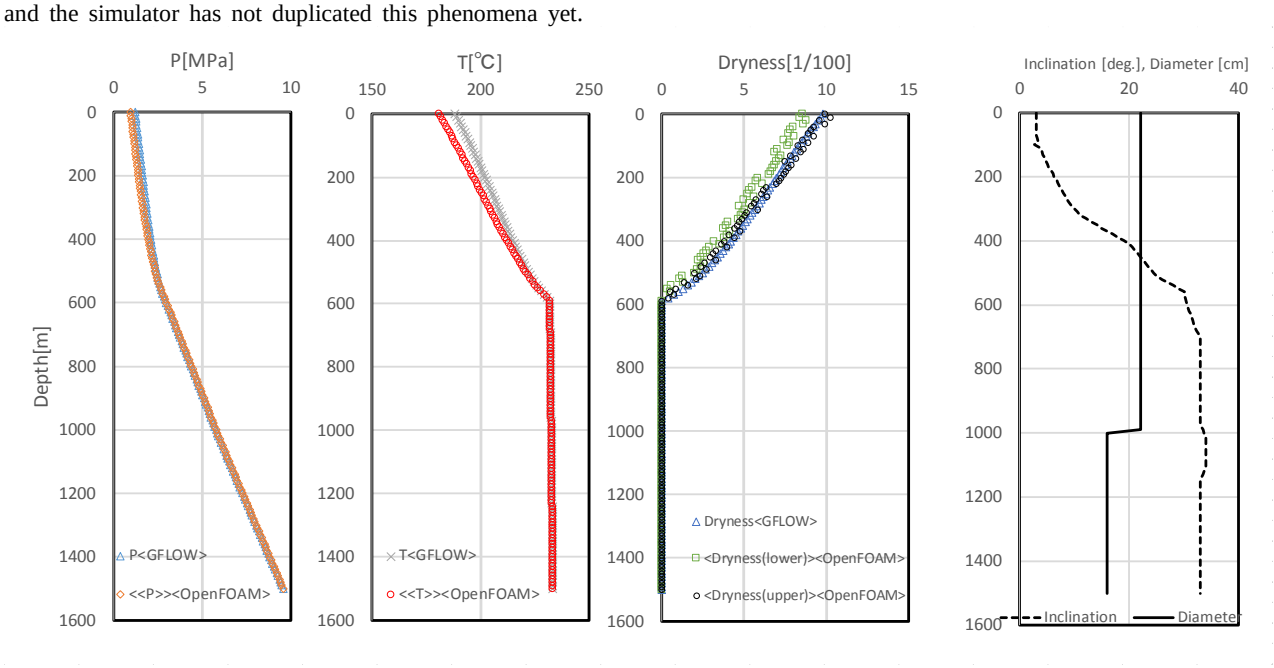

Figure 19: Comparison of GFLOW and OpenFOAM 3D-CFD in case of a deviated production well in Japan.

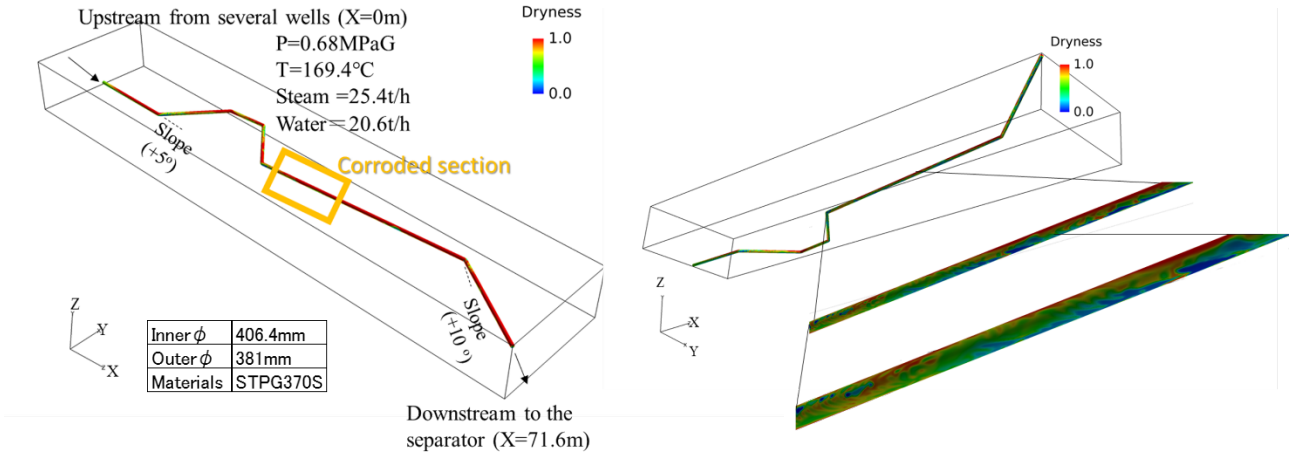

Figure 20: OpenFOAM 3D-CFD result (inner face Dryness of the pipeline) simulated a surface two-phase flow pipeline with some bending parts and slope (5-10 degrees) in Japan. (Left: Birds-eye view from top, Right: Birds-eye view from bottom)

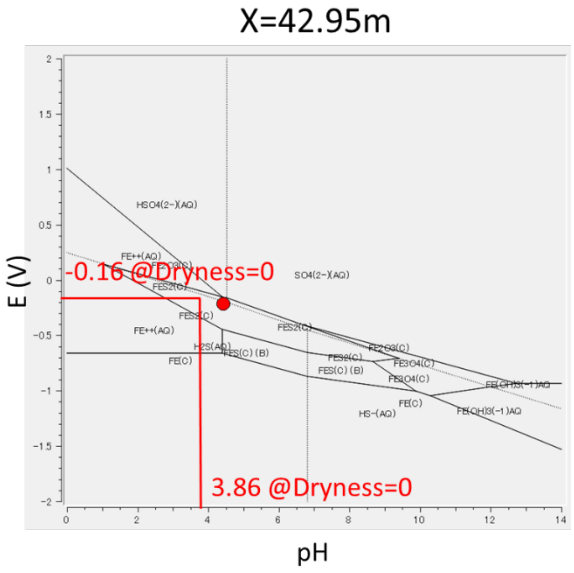

Figure 22: Pourbaix diagrams of H2S-H2O-Fe system (at x=42.95m)

5. CONCLUSION

We discussed recent attempts of comparison between computed models and field data to predict the corrosion and scaling problems of geothermal production wells and pipelines using OpenFOAM 3D-CFD and WellCHEM. By comparison of OpenFOAM 3D-CFD and Gflow at a deviated production well, we could ger harmotic result. By comparison of OpenFOAM 3D-CFD and WellCHEM at a surface two-phase flow pipeline in Japan, we found out some computed differences between two codes in two phase condition but OpenFOAM 3D-CFD could explain the phenomena of inhomogineous dryness wellbore condition at a deviated production well. If inhomogeneous water phase area traps the majority of dissolved chemicals, corrosion and scaling will be accelerated in this section. In case of a surface two-phase flow pipeline, coupled analysis using OpenFOAM 3D-CFD and WellCHEM could get harmonic result to the field observation result.

ACKNOWLEDGEMENTS

I would like to thank K.Lihiti of Quest Integrity NZ for useful discussion regarding the concept of this study. I am grateful to J. Burnell of GNS Science who has developed WellCHEM Code jointly with us.

This research project “Research and Development of Geothermal Power Generation Technology/Innovative Technology Development for Promotion of Introduction of Geothermal Power Plant/Development of Geothermal Power Plant Risk Assessment System (Prediction, Measure and Management for Scale and Corrosion)” (FY2014-FY2017, Co-researcher: GERD, AIST, and NKKT) is supported by New Energy and Industrial Technology Development Organization (NEDO).

REFERENCES

Aunzo, Z. P., Bjornsson, G., Bodvarsson, G. S.: Wellbore Models GWELL, GWNACL, and HOLA User’s Guide. Earth Sciences Division, Lawrence Berkeley Laboratory Report. No. LBL-31428. (1991).

Jasak, H., Jemcov, A., and Tukovic, Z.: OpenFOAM: A C ++ Library for Complex Physics Simulations, International Workshop on Coupled Methods in Numerical Dynamics, volume m, (2007), 1–20.

Kato, M. , Okobe, T., Nakata, H., Kissling, W. and White, S. P.: Development of a wellbore flow simulator GFLOW, Proc Ceoth res Soc, Japan, A18 (2001)(in Japanese).

Kato, M., Okabe, T., Ujyo, S. Takanashi, K., Kunzman, R.: Development of Wellbore Simulator and Verification Test of High Temperature PTS+FLUID Sampler Logging System for a Highly Deviated Geothermal Well, Proc. World Geothermal Congress 2015 Melbourne, Australia, 19-25 April 2015,

Lichti, K.A., White, S.P., McGavin, P.: Software for Geothermal Corrosion and Risk Based Assessment, Proc. World Geothermal Congress 2005, Antalya, Turkey. (2005).

Miller, C.W.: Numerical Model of Transient Two-Phase Flow in a Wellbore, Lawrence Berkeley Laboratory, LBL-9056. (1979).

Sato, M., Okabe, T., Nakata, H., Yanagisawa, N., Kawasaki, K. Sampler test at the Hijiori site and evaluation of Anhydrite scale. Proc. Annual Meeting Geothermal Research Society of Japan 2003, 26, (2003), (in Japanese).

White, S. P., Lichti, K. A. and Bacon, L. G.: Application of Chemical and Wellbore Modelling to the Corrosion and Scaling Properties of Ohaaki Deep Wells, Proc World Geothermal Congress, Kyushu, Tohoku, Japan, (2000), 3963-3967